

Simulation of electronic and optical properties of ZnO/MgZnO quantum dot laser

S. TALEB*, B. SOUDINI, I. LAGRAA, H. ABID

Applied Materials Laboratory (AML), University of Sidi Bel Abbès, Sidi Bel Abbès, Algeria

In this work we report a modeling and numerical simulation of the carrier dynamics of ZnO/MgZnO of quantum dot lasers (QDLs). Our calculations are carried out by solving the set of seven rate equations for carriers and photons at four energy states using the fourth order of Runge-Kutta method in MATLAB software. Many properties of QDLs such as the photon density, output power and the small signal modulation response versus the time and injection current have been studied and discussed for the ground state (GS), first excited state (ES1), and second excited state (ES2). The modeling simulation validity is verified by comparison with other works. This work shows the advantage of ZnO/MgZnO QDLs to enhance the properties of laser.

(Received October 25, 2017; accepted April 8, 2019)

Keywords: Quantum dot laser, ZnO/MgZnO, Rate equations model

1. Introduction

Quantum dot (QD) is a semiconductor-based structure where the excitons are strongly confined in the three dimensions of space (3D), which induces a finer state density than in conventional structures. Discrete levels are created in QD by this confinement, that gives the QD properties similar to those of an atom, so we can consider the QDs as artificial atoms [1]. Until the mid 1980s, lasers with a thick active region of several microns were dominated the market. But it was only with the introduction of quantum well laser diodes and the sharp reduction in threshold current densities of the order of 40 to 50 A / cm² [2], obtained first by ZI Alferov, Nobel Prize in 2000, and the market for laser diodes exploded. In 1982, Y. Arakawa and H. Sakaki [3], of the University of Tokyo, theoretically studied the 3D confinement effect in the active area of QDs. QDLs have attracted much attention in recent years [4-6] because they present an excellent properties such as lower transparency current density [7], temperature insensitivity [8], high material gain [9], as well as high differential gain [10-11], and reduced linewidth enhancement factor (LEF or αH -factor) at the lasing wavelength [12]. These superiorities mentioned of QDLs make them attractive configurations to be employed on the laser and communications promising optical fibers devices.. Among the wide-gap semiconductors that received great attention in the last years, Zinc Oxide (ZnO) and its ternary alloys. ZnO is an II-VI compound semiconductor with a hexagonal wurtzite structure. In the last few years, ZnO gets much attention for its application in various fields such as in the area of green, blue, and ultraviolet (UV) light-emitting diodes (LEDs), semiconductor optical amplifier (SOA), and lasers [13-16], transparent high power electronics, optical waveguides and solar cells [17-18]. In addition, their potential advantages over III-V nitrides, such as substrate

availability, comparatively simpler growth and processing technologies, and larger exciton binding energy (60 meV against 25 meV for GaN) [19-20] even at room temperature which promotes the excitonic recombination [21].

In this paper, ZnO/Mg_{0.3}Zn_{0.7}O QDs are considered as an active region in a QD laser consisting of four energy levels for confined carriers. We assumed that all QDs are uniform according to the theoretical and experimental studies performed in references [22-24]. We have considered lens-shape ZnO QDs of diameter D=20 nm, height H=10 nm, and an MgZnO wetting layer of a thickness of 1 nm. In our study, we assumed that QDs are spaced enough to avoid the quantum tunneling effects, and the homogeneous and inhomogeneous effects are ignored. The QD include three energy states with two-fold degenerate ground state (GS) and double four-fold degenerate excited state (ES1, ES2). The numerical model used for ZnO/MgZnO QDL is based on a set of coupled rate equations, which consists of four energy states where three of them are joined in lasing. We used the 4th order of Runge-Kutta method in MATLAB software, to extract the laser characteristics such as output power-current (P-I), gain, time variation of the photon densities, the output power and the intensity modulation response.

2. Theoretical model

We have considered four energy levels which are belong to wetting layer (WL), second and first excited states (ES2) and (ES1), and the ground state (GS). The energy levels of the active region in QD laser for conduction band are shown in Fig.1. Fig. 1 shows the principle carrier dynamics in the conduction band as the cascade relaxation model of ZnO/MgZnO. The carriers are injected directly into the tank of the WL creating

consequently an injection current I . A portion of the pairs electron-hole created is captured on the second ES2 with a time of relaxation (τ_{WL-ES2}) while the other part recombines spontaneously. The carriers occupying the ES2 can then relax on ES1, escape into the tank of wetting layer (τ_{ES2-WL}) or recombine radiatively. The carriers already relaxed on ES1 can be released on the excited state ($\tau_{ES1-ES2}$), recombine spontaneously or relax on the

ground state GS (τ_{ES1-GS}). A part of these last reissued carriers on the excited state (τ_{GS-ES1}), and the rest perform decay due to the spontaneous and Auger effects (τ_r), or contribute in stimulated recombination and generate laser photons (through the analysis of carrier dynamics within the QD).

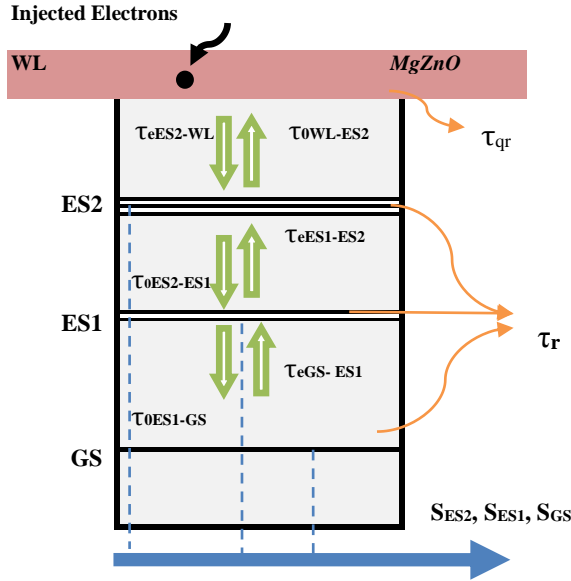


Fig. 1. Energy diagram of the laser active region of MgZnO/ZnO with the diffusion, recombination, and relaxation processes.

The QD laser numerical model is based on the seven coupled rate equations, through an analysis of carrier dynamics inside the QD. This model is divided into two types of equations: the first for electrons and the second for photons. The rate equations can be written as follow [25-26]:

$$\frac{dS_{GS}}{dt} = -\frac{S_{GS}}{\tau_s} + \Gamma v_g g_{GS} (2f_{GS} - 1) S_{GS} + \beta_{sp} \frac{N_{GS}}{\tau_{sp}} \quad (1)$$

$$\frac{dS_{ES1}}{dt} = -\frac{S_{ES1}}{\tau_s} + \Gamma v_g g_{ES1} (2f_{ES1} - 1) S_{ES1} + \beta_{sp} \frac{N_{ES1}}{\tau_{sp}} \quad (2)$$

$$\frac{dS_{ES2}}{dt} = -\frac{S_{ES2}}{\tau_s} + \Gamma v_g g_{ES2} (2f_{ES2} - 1) S_{ES2} + \beta_{sp} \frac{N_{ES2}}{\tau_{sp}} \quad (3)$$

$$\begin{aligned} \frac{dN_{GS}}{dt} = & -\frac{N_{GS}}{\tau_r} - \Gamma v_g g_{GS} (2f_{GS} - 1) S_{GS} - \frac{N_{GS}}{\tau_{eGS}} (1 - f_{ES1}) \\ & + \frac{N_{ES1}}{\tau_{0ES1-GS}} (1 - f_{GS}) \end{aligned} \quad (4)$$

$$\begin{aligned} \frac{dN_{ES1}}{dt} = & -\frac{N_{ES1}}{\tau_r} - \Gamma v_g g_{ES1} (2f_{ES1} - 1) S_{ES1} + \frac{N_{GS}}{\tau_{eGS}} (1 - f_{ES1}) \\ & - \frac{N_{ES1}}{\tau_{0ES1-GS}} (1 - f_{GS}) + \frac{N_{ES2}}{\tau_{eES2-ES1}} (1 - f_{ES1}) - \frac{N_{ES1}}{\tau_{eES1}} (1 - f_{ES2}) \end{aligned} \quad (5)$$

$$\begin{aligned} \frac{dN_{ES2}}{dt} = & -\frac{N_{ES2}}{\tau_r} - \Gamma v_g g_{ES2} (2f_{ES2} - 1) S_{ES2} - \frac{N_{ES2}}{\tau_{eES2}} \\ & + \frac{N_{WL}}{\tau_c} (1 - f_{ES2}) - \frac{N_{ES2}}{\tau_{0ES2-ES1}} (1 - f_{ES1}) + \frac{N_{ES1}}{\tau_{eES1}} (1 - f_{ES2}) \end{aligned} \quad (6)$$

$$\frac{dN_{WL}}{dt} = n_i \frac{I}{q} - \frac{N_{WL}}{\tau_{qr}} + \frac{N_{ES2}}{\tau_{eES2}} - \frac{N_{WL}}{\tau_c} (1 - f_{ES2}) \quad (7)$$

where N_{WL} , N_{ES2} , N_{ES1} , and N_{GS} are carrier densities in WL and the discrete levels of the quantum dot ES2, ES1 and GS, respectively. S_{ES2} , S_{ES1} , and S_{GS} show the density of photons in ES2, ES1 and GS, respectively. The

terms $-\frac{S_{ES2}}{\tau_s}$, $-\frac{S_{ES1}}{\tau_s}$, and $-\frac{S_{GS}}{\tau_s}$ represent photon decay rates in ES2, ES1 and GS, respectively. In these terms, τ_s^{-1} is the photon lifetime and it is given by

$$\tau_s^{-1} = c / n_r (\alpha + \ln(1/R_1 R_2) / 2L) \quad (8)$$

where n_r is the refractive index of the active region, α is the internal loss of cavity, R_1 and R_2 are the cavity mirror reflectivity's, L is the cavity length, and c is the speed of light.

$\beta_{sp} N_m / \tau_{sp}$ indicates the photon generation rates provided by spontaneous recombination in the level m ($m=GS$, ES1 or ES2), with β_{sp} is spontaneous emission coupling factor, and τ_{sp} is spontaneous recombination time. $\Gamma v_g g_{GS} (2f_{GS} - 1) S_{GS}$ and $\Gamma v_g g_{ES1/ES2} (2f_{ES1/ES2} - 1) S_{ES1/ES2}$ define photon generation rate and carrier decay rate due to stimulated emission, where Γ is optical confinement factor, v_g is group velocity, and g_m is gain of level m which is given by

$$g_m = \frac{k_m}{1 + \delta_m S_m} \quad (9)$$

with δ_m is the gain factor written by

$$\delta_m = \frac{q^2 p_{cv}^2 \tau_s \Gamma}{4\hbar V_a n_r m_0^2 \delta_0 E_m \Gamma_{hom}} \quad (10)$$

and

$$k_m = \frac{2\pi q^2 \hbar \mu_m \xi p_{cv}^2}{c n_r m_0^2 \delta_0 V_d \gamma_0 E_m} \quad (11)$$

where γ_0 is the inhomogeneous broadening coefficient and ξ is the coverage of dots given by $\xi = N_d V_d$ with N_d is the dot density, and V_d is the dot volume $V_d = 2\pi(D/2)^2 H/3$.

In the expression of gain factor, V_a is the active region volume and Γ_{hom} is the homogeneous broadening. The square of transition matrix element is given as $|p_{cv}|^2 = |I_{cv}|^2 M^2$, where I_{cv} represents the overlap

integral between the envelope functions of an electron and a hole, and $M^2 = \frac{m_e^2 E_g (E_g + \Delta)}{12m_e (E_g + 2\Delta/3)}$ with E_g is the band gap, m_e is the electron effective mass, Δ is the spin-orbit interaction energy of the QD material. The terms $-\frac{N_m}{\tau_r}$ and $-\frac{N_{WL}}{\tau_{qr}}$ are decay rates of carrier density in level m and WL, respectively, $-N(1-f)/\tau_e$ indicate to the carrier escape rate from the current level to higher level, and τ_e is carrier escape time. By the same, $N(1-f)/\tau_0$ and $-N(1-f)/\tau_0$ are carrier relaxation rates from higher level to current level and from current level to lower level, respectively. τ_0 , is the relaxation time. In addition, $\frac{N_{WL}}{\tau_c}(1-f_{ES2})$ means the carrier capture rate from WL to ES2, where τ_c is carrier capture time. We define f_m as carrier occupation probability of level m (effect Pauli-blocking principle on the carriers transfer from one level to another), with $f_m = N_m / \mu_m N_D$, N_D represents the total number of QDs, and μ_m represents degeneracy of level m . By definition n_i as coefficient of injected current rate, I pumping current and q is unit charge. The expression of the different relaxation times is written as follows:

$$\tau_{eGS} = \mu_{ES1} / \mu_{GS} \tau_{ES1-GS} e^{(E_{ES1}-E_{GS}/k_B T)} \quad (12)$$

$$\tau_{eES1} = \mu_{ES2} / \mu_{ES1} \tau_{ES2-ES1} e^{(E_{ES2}-E_{ES1}/k_B T)} \quad (13)$$

$$\tau_{ES1-GS} = \tau_{0ES1-GS} / 1 - f_{GS} \quad (14)$$

$$\tau_{ES2-ES1} = \tau_{0ES2-ES1} / 1 - f_{ES1} \quad (15)$$

The parameters related to the bulk materials applied and all parameters used in our simulation are listed in Tables 1 and 2, respectively.

Table 1. ZnO and MgO parameters used in the present work

	a (Å)	c(Å)	Eg (eV)	b (eV)	m _e	ε ₀	Δ _{so(me)}	Δ _{cr(me)}
ZnO	3.25 [27]	5.205 [27]	3.37 [28]	--	0.23m ₀ [27]	8.1 [29]	13.59 [27]	38 [27]
MgO	3.199 [30]	4.11 [31]	5.289 [32]	0.87 [32]	0.28m ₀ [33]	9.6 [34]	32.169 [35]	317.2 [35]

Table 2. Some parameters used in the simulation

Symbols	Definitions	Values
Carrier injection rate	n_i	0.9
Optical confinement factor	Γ	0.01
Spontaneous emission coupling factor	β_{sp}	1×10^{-4}
Optical loss	α_l	$6 \times 10^2 \text{ m}^{-1}$
Cavity's reflectivity of mirrors	R_1, R_2	0.3
Decay time in WL	τ_{qr}	$5 \times 10^{-9} \text{ s}$
Decay time in es2 ES1 GS	τ_r	$5 \times 10^{-9} \text{ s}$
Carrier capture time from WL to ES2	τ_c	$2 \times 10^{-12} \text{ s}$
Relaxation from ES2 to ES1	$\tau_{0\text{ES2-ES1}}$	$2 \times 10^{-12} \text{ s}$
Relaxation time for ES1 to GS	$\tau_{0\text{ES1-GS}}$	$12 \times 10^{-12} \text{ s}$
Spontaneous recombination time	τ_{sp}	$5 \times 10^{-10} \text{ s}$
Degeneracy	$\mu_{GS}, \mu_{ES1}, \mu_{ES2}$	2, 4, 6
Cavity width	w	$1 \times 10^{-5} \text{ m}$
Active region length	L	$15 \times 10^{-4} \text{ m}$
Homogenous broadening factor	Γ_{hom}	$1 \times 10^{-2} \text{ eV}$
Inhomogeneous broadening factor	γ_0	$2 \times 10^{-2} \text{ eV}$
Energy Separation ES2-ES1	$E_{ES2} - E_{ES1}$	0.058 eV
Energy Separation ES1-GS	$E_{ES1} - E_{GS}$	0.053 eV

To study the modulation of response QDL, the rate equations are linearized by a modified small-signal analysis [36]. Considering I , N_n ($n = \text{WL}$ or ES1 or ES2 or GS) and S_m as dynamic variables and in order to simplify the model, g_m are assumed to be constant. The current modulation and the corresponding carrier and photon variations are as follows:

$$\begin{aligned} I(t) &= I_i e^{J \omega t} \\ N_n(t) &= N_{n,1} e^{J \omega t} \\ S_m(t) &= S_{m,1} e^{J \omega t} \end{aligned} \quad (16)$$

where ω is the modulation frequency.

Using (12) in the differential rate equations, we obtain the matrix A:

$$A = \begin{bmatrix} A11 + J \omega & 0 & 0 & A14 & 0 & 0 & 0 \\ 0 & A22 + J \omega & 0 & 0 & A25 & 0 & 0 \\ 0 & 0 & A33 + J \omega & 0 & 0 & A36 & 0 \\ A41 & 0 & 0 & A44 + J \omega & A45 & 0 & 0 \\ 0 & A52 & 0 & A54 & A55 + J \omega & A56 & 0 \\ 0 & 0 & A63 & 0 & A65 & A66 + J \omega & A67 \\ 0 & 0 & 0 & 0 & 0 & A76 & A77 + J \omega \end{bmatrix}$$

$$A * \begin{bmatrix} S_{GS,1} \\ S_{ES1,1} \\ S_{ES2,1} \\ N_{GS,1} \\ N_{ES1,1} \\ N_{ES2,1} \\ N_{WL,1} \end{bmatrix} = \frac{n_i I_1}{q} \begin{bmatrix} 0 \\ 0 \\ 0 \\ 0 \\ 0 \\ 0 \\ 1 \end{bmatrix} \quad (17)$$

with

$$\begin{aligned} A11 &= -\frac{1}{\tau_s} - \Gamma v_g g_{GS} (2f_{GS} - 1), & A14 &= -\frac{\beta_{sp}}{\tau_{sp}} - \frac{2\Gamma v_g g_{GS}}{\mu_{GS} N_D} S_{GS}, & A22 &= -\frac{1}{\tau_s} - \Gamma v_g g_{ES1} (2f_{ES1} - 1), \\ A25 &= -\frac{\beta_{sp}}{\tau_{sp}} - \frac{2\Gamma v_g g_{ES1}}{\mu_{ES1} N_D} S_{ES1}, & A33 &= \frac{1}{\tau_s} - \Gamma v_g g_{ES2} (2f_{ES2} - 1), & A36 &= -\frac{\beta_{sp}}{\tau_{sp}} - \frac{2\Gamma v_g g_{ES2}}{\mu_{ES2} N_D} S_{ES2}, \\ A41 &= \Gamma v_g g_{GS} (2f_{GS} - 1), & A44 &= \frac{1}{\tau_r} + \frac{2\Gamma v_g g_{GS}}{\mu_{GS} N_D} S_{GS} + \frac{(1 - f_{ES1})}{\tau_{eGS}} + \frac{1}{\tau_{0\text{ES1-GS}}} \frac{1}{\mu_{GS} N_D} N_{ES1}, \end{aligned}$$

$$\begin{aligned}
A45 &= -\frac{N_{GS}}{\tau_{eGS}\mu_{ES1}N_D} - \frac{1-f_{GS}}{\tau_{0ES1-GS}}, & A52 &= \Gamma v_g g_{ES1} (2f_{ES1} - 1), & A54 &= -\frac{(1-f_{ES1})}{\tau_{eGS}} + \frac{N_{ES1}}{\tau_{0ES1-GS}\mu_{GS}N_D}, \\
A55 &= \frac{1}{\tau_r} + \frac{2\Gamma v_g g_{ES1}}{\mu_{ES1}N_D} S_{ES1} + \frac{N_{GS}}{\tau_{eGS}\mu_{ES1}N_D} + \frac{1-f_{GS}}{\tau_{0ES1-GS}} + \frac{N_{ES2}}{\tau_{eES2-ES1}\mu_{ES1}N_D} + \frac{1-f_{ES2}}{\tau_{eES1}}, \\
A56 &= -\frac{1-f_{ES1}}{\tau_{eES2-ES1}} - \frac{N_{ES1}}{\tau_{eES1}\mu_{ES2}N_D}, & A63 &= \Gamma v_g g_{ES2} (2f_{ES2} - 1), & A65 &= -\frac{N_{ES2}}{\tau_{0ES2-ES1}\mu_{ES1}N_D} - \frac{1-f_{ES2}}{\tau_{eES1}}, \\
A66 &= \frac{1}{\tau_r} + \frac{2\Gamma v_g g_{ES2}}{\mu_{ES2}N_D} S_{ES2} + \frac{1}{\tau_{eES2}} + \frac{N_{WL}}{\tau_{c\mu_{ES2}N_D}} + \frac{1-f_{ES1}}{\tau_{0ES2-ES1}} + \frac{N_{ES1}}{\tau_{eES1}\mu_{ES2}N_D}, & A67 &= -\frac{1-f_{ES2}}{\tau_c}, \\
A76 &= -\frac{1}{\tau_{eES2}} - \frac{N_{WL}}{\tau_c\mu_{ES2}N_D}, & A77 &= \frac{1}{\tau_{qr}} + \frac{1-f_{ES2}}{\tau_c}
\end{aligned}$$

To obtain the small signal carrier in each state, we can apply the *Cramer rule* as follows

$$S_{GS,1} = \frac{\begin{vmatrix} 0 & 0 & 0 & A14 & 0 & 0 & 0 \\ 0 & A22+J\omega & 0 & 0 & A25 & 0 & 0 \\ 0 & 0 & A33+J\omega & 0 & 0 & A36 & 0 \\ 0 & 0 & 0 & A44+J\omega & A45 & 0 & 0 \\ 0 & A52 & 0 & A54 & A55+J\omega & A56 & 0 \\ 0 & 0 & A63 & 0 & A65 & A66+J\omega & A67 \\ \frac{n_i I_l}{q} & 0 & 0 & 0 & 0 & A76 & A77+J\omega \end{vmatrix}}{\det A},$$

$$S_{ES1,1} = \frac{\begin{vmatrix} A11+J\omega & 0 & 0 & A14 & 0 & 0 & 0 \\ 0 & 0 & 0 & 0 & A25 & 0 & 0 \\ 0 & 0 & A33+J\omega & 0 & 0 & A36 & 0 \\ A41 & 0 & 0 & A44+J\omega & A45 & 0 & 0 \\ 0 & 0 & A54 & A55+J\omega & A56 & 0 & 0 \\ 0 & 0 & A63 & 0 & A65 & A66+J\omega & A67 \\ 0 & \frac{n_i I_l}{q} & 0 & 0 & 0 & A76 & A77+J\omega \end{vmatrix}}{\det A},$$

$$S_{ES2,1} = \frac{\begin{vmatrix} A11+J\omega & 0 & 0 & A14 & 0 & 0 & 0 \\ 0 & A22+J\omega & 0 & 0 & A25 & 0 & 0 \\ 0 & 0 & 0 & 0 & 0 & A36 & 0 \\ A41 & 0 & 0 & A44+J\omega & A45 & 0 & 0 \\ 0 & A52 & 0 & A54 & A55+J\omega & A56 & 0 \\ 0 & 0 & 0 & 0 & A65 & A66+J\omega & A67 \\ 0 & 0 & \frac{n_i I_l}{q} & 0 & 0 & A76 & A77+J\omega \end{vmatrix}}{\det A}$$

With $\det A$ is the determinant of the matrix A.

3. Simulation results and discussions

Fig. 2 shows the dynamic behavior of the photons of ZnO/MgZnO QD laser for three levels of QD (GS, ES1 and ES2) with various injected currents ($I = 0.01, 0.02, 0.03$ and 0.05 A). From this figure we can see that the time delay decreases with the increase of the pumping current. This variation means that the effective carrier lifetime is reduced [37]. This analysis is clearer in Fig. 3, which represents photon density as a function of electron density

of GS. As shown in Fig. 2 a, b, and c, the photon density for the three levels increases until stable states. Before this stability we can see rating relaxation oscillations in the early stages of flow of injection. This is due to additional carriers created by the injection current inside quantum dots. Moreover, when we increase the intensity of injection current, the threshold current decreases. We also note that the intensity of the photon generated at the GS level is higher than at ES1 and ES2.

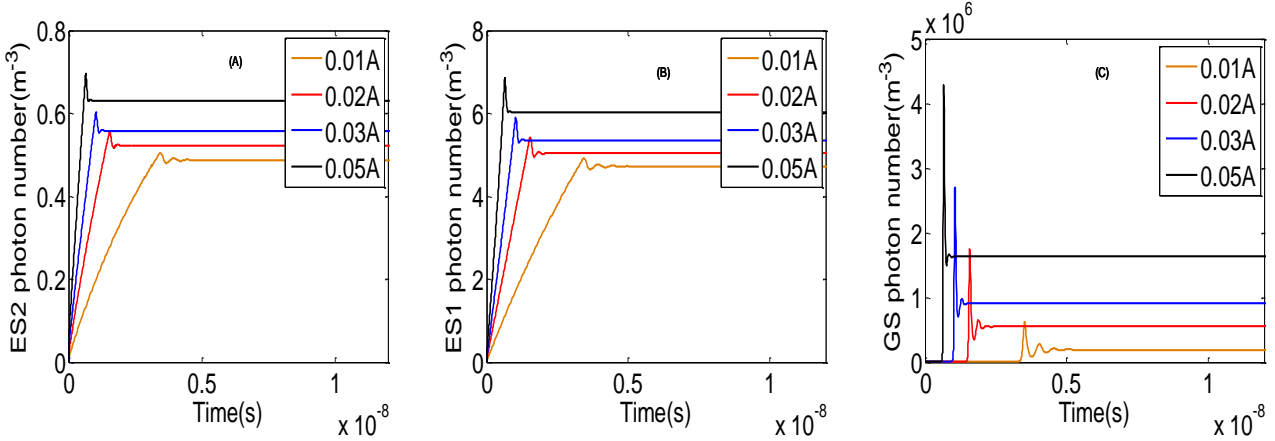


Fig. 2. Time variation of photon density for the (A) ES2, (B) ES1 and (C) GS states for different injection currents $I=0.01, 0.02, 0.03$, and 0.05 A .

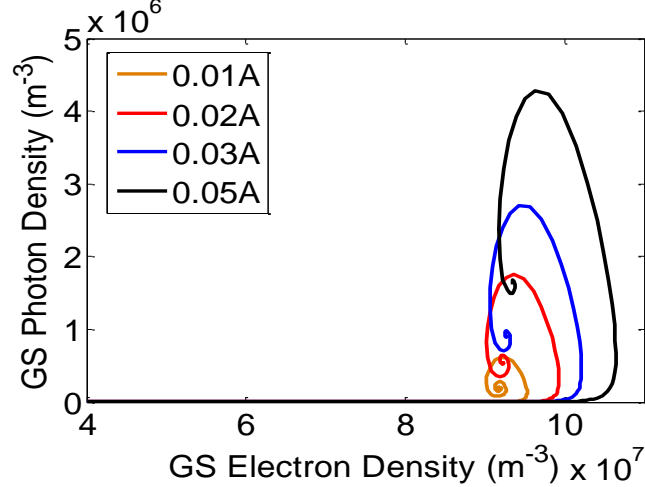


Fig. 3. Photon density vs. electron density of GS

3.1. Output power

The output power of different states m is given by:

$$\mathbf{P}_{\text{out}-m} = \mathbf{S}_m \mathbf{E}_m / \tau_s \quad (18)$$

Fig. 4 exhibits the output power of ZnO/MgZnO QD laser for three discrete levels (GS, ES1 and ES2) as a function of time for different injected current ($I = 10, 20, 30$ and 50 mA). It was clear that the structure presents a higher output power at GS level (Fig. 4 c) than the others levels (Fig. 4 a and b) whatever the value of the injected

current I . in the three parts the value of the power is directly proportional to the intensity of the injection. On the other hand, we can observe that the switching times decrease with the increase of current injection.

After the current injection, the carriers of GS start to emit photons until the GS related emission output gets saturation. At this moment, the carriers of ES1 emit photons similarly until the saturation and then ES2 starts emission. Fig. 5 displays the output power characteristic curve versus injection currents where we have considered the threshold current I_{th} equals to $10^{13}, 0.56$ and 4.1 A for the GS, ES1 and ES2, respectively.

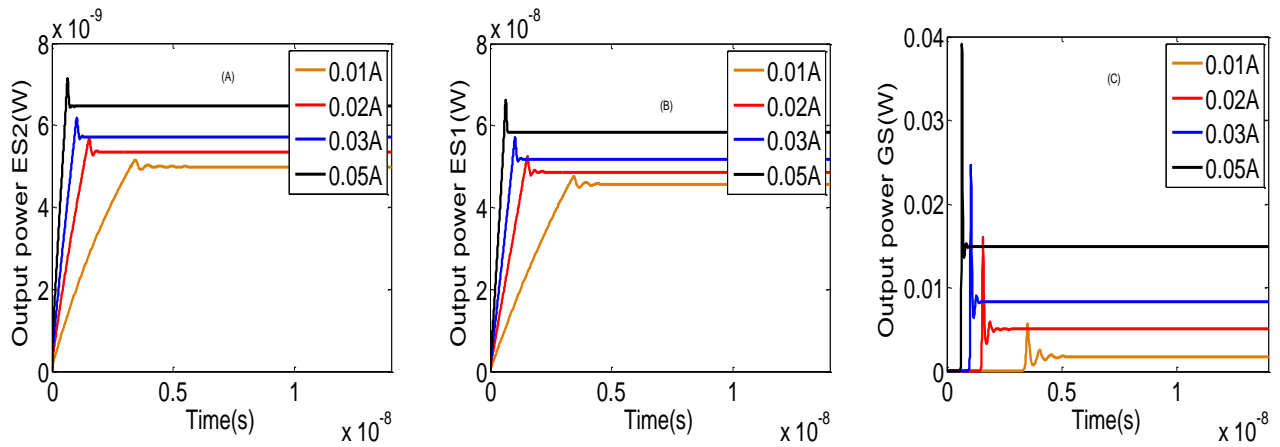


Fig. 4. Laser output power vs. time for the (a) ES2, (b) ES2 and (c) GS states for different injection currents $I = 0.01, 0.02, 0.03, \text{ and } 0.05 \text{ A}$

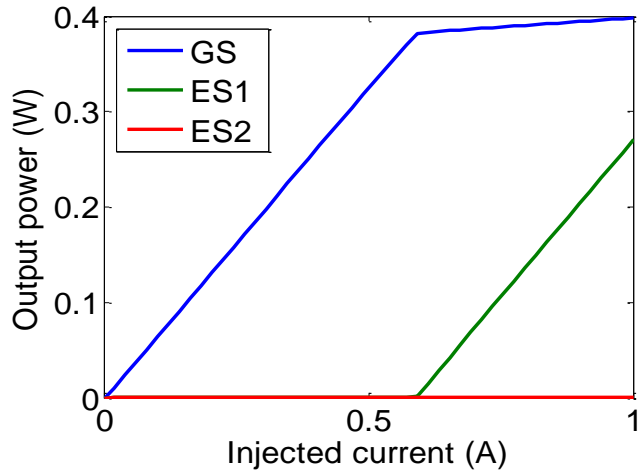


Fig. 5. Output power characteristic curve vs. injection currents

3.2. Optical gain

The optical gain for different levels m is written:

$$Gain_m = \frac{\Gamma K_m \left(\frac{2N_m}{\mu_m N_D} - 1 \right)}{1 + \delta_m S_m} \quad (19)$$

Fig. 6 shows the gain characteristic versus injection currents for the three energy states (GS, ES1 and ES2). At low currents, we notice that the gain is negative for all three energy levels where the GS state reached the saturation of about $\sim 2 \times 10^4 \text{ cm}^{-1}$ before the ES1 and ES2 levels.

Fig. 7 represents the low signal modulation response versus modulation frequency under the effect of injected current I ($I=0.01, 0.02, 0.03 \text{ and } 0.05 \text{ A}$) for GS, ES1, and ES2 states. It can be seen that the increase of the current injection leads to a 3dB modulation bandwidth for the

three levels. The optical power inside the cavity boots with injection current, which produces a higher relaxation frequency and therefore the bandwidth modulation, is extended.

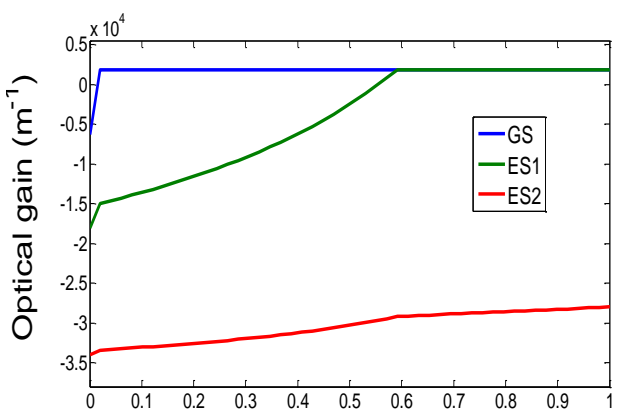


Fig. 6. Gain characteristic curve vs. injection currents

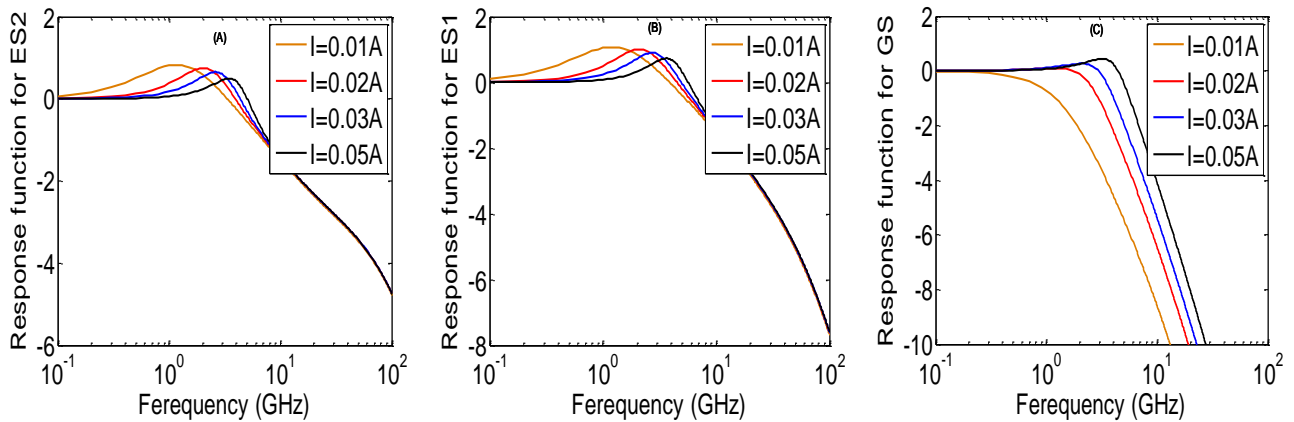


Fig. 7. Small signal modulation response at various injection currents I for (A) ES, (B) ES2, and (C) GS states

4. Conclusion

In this paper, the internal mechanism of ZnO/MgZnO QDL has been numerically modeled and simulated. Our results have shown that by increasing the injection current, the switching-on and stability time decrease. Furthermore, the threshold currents and the photon densities for three levels (GS, ES1 and ES2) increase until get saturation. The immediate consequence of this resulting effect is the higher relaxation frequency and therefore the extension of the bandwidth modulation. Finally, the obtained results show that ZnO/MgZnO QDL presents promising properties compared to those obtained for InAs/GaAs [25].

Acknowledgements

The research contained in this paper has been supported by the Applied Material Laboratory (AML), university Research center, University Djillali Liabes of Sidi BelAbbes, Algeria.

References

- [1] T. Steiner, Sensor Review **24**(3), 320 (2004).
- [2] Z. I. Alferov, S. V. Ivanov, P. S. Kopev, N. N. Ledentsov, M. E. Lutsenko, M. I. Nemenov, B. Y. Meltsner, V. M. Ustinov, S. V. Shaposhnikov, Sov. Phys. Semicond. **24**, 92 (1990).
- [3] Y. Arakawa, H. Sakaki, Appl. Phys. Lett. **40**, 939 (1982).
- [4] E. U. Rafailov, M. A. Cataluna, E. A. Avrutin, Physics and Devices, Wiley, New York, 2011.
- [5] M. Sugawara, R. K. Willardson, E. R. Weber, Semiconductors and Semimetals, Academic Press (1999).
- [6] M. Gioannini, A. Sevega, I. Montrosset, Opt. Quantum Electron **38**(4), 381 (2006).
- [7] G. T. Liu, A. Stintz, H. Li, K. J. Malloy, L. F. Lester, Electron. Lett. **35**(14), 1163 (1999).
- [8] S. S. Mikhlin, A. Kovsh, I. Krestnikov, A. Kozhukhov, D. Livshits, N. Ledentsov, Y. M. Shernyakov, I. Novikov, M. Maximov, V. Ustinov, Semicond Sci Technol. **20**(5), 340 (2005).
- [9] M. V. Maximov, N. N. Ledentsov, Nanoscience and Nanotechnology, CRC Press, 3109 (2004).
- [10] P. Bhattacharyya, A. A. Avrutin, A. C. Bryce, J. H. Marsh, D. Bimberg, F. Heinrichsdorff, V. M. Ustinov, S. V. Zaitsev, N. N. Ledentsov, P. S. Kopev, Z. I. Alferov, A. I. Onischenko, E. P. O'Reilly, IEEE J. Sel. Top. Quantum Electron. **5**(3), 648 (1999).
- [11] P. Bhattacharya, D. Klotzkin, O. Qasaimeh, W. Zhou, S. Krishna, D. Zhu, IEEE J. Sel. Top. Quantum Electron **6**(3), 426 (2000).
- [12] M. T. Crowley, N. A. Naderi, H. Su, F. Grillot, L. F. Lester, Laser, Semiconductors and Semimetals: Advances Semiconductor Lasers **86**, 371 (2012).
- [13] S. Kalusniak, S. Sadofev, J. Puls, F. Hannenberger, Laser Photon. Rev. **3**, 233 (2009).
- [14] Y. S. Choi, J. W. Kang, D. K. Hwang, S. J. Park, IEEE Trans. Electron. Dev. **57**(1), 26 (2010).
- [15] M. A. Al-Mossawi, A. G. Al-Shatravi, A. H. Al-Khursan, Insciences J. **2**, 52 (2012).
- [16] M. Abdullah, A. H. Al-Khursan, R. A. Al-Ansari, Recent Patents on Electrical Engineering **2**, 226 (2009).
- [17] S. J. Pearton, D. P. Norton, K. Ip, Y. W. Heo, T. Steiner, Superlattices Microstruct. **34** (1-2), 3 (2003).
- [18] W. W. Wenas, A. Yamada, K. Takahashi, M. Yoshino, M. Konagai, J. Appl. Phys. **70**, 7119 (1991).
- [19] Z. K. Tang, G. K. L. Wong, P. Yu, M. Kawasaki, A. Ohtomo, H. Koinuma, Y. Segawa, Appl. Phys. Lett. **72**, 3270 (1998).
- [20] B. K. Sonawane, M. P. Bhole, D. S. Patil, Optoelectron. Adv. Mat. **2**(11), 714 (2008)
- [21] T. Makino, C. H. Chia, N. T. Tuan, H. D. Sun, Y. Segawa, M. Kawasaki, A. Ohtomo, K. Tamura, H. Koinuma, Appl. Phys. Lett. **77**, 975 (2000).
- [22] M. Gioannini, IEEE Journal of Quantum Electronics **42**(3), 331 (2006).

- [23] M. Zieliński, M. Korkusiński, P. Hawrylak, Physical Review B **81**(8), 085301 (2010).
- [24] H. Jiang, J. Singh, Applied Physics Letters **71**(22), 3239 (1997).
- [25] S. F. Lv, I. Montrosset, M. Gioannini, S. Song, J. Ma, Optoelectronics Letters **7**(2), 122 (2011).
- [26] M. Sugawara, K. Mukai, Y. Nakata, H. Ishikawa, A. Sakamoto, Physical Review B **61**, 7595 (2000).
- [27] W. Lambrecht, A. V. Rodina, S. Limpijumnong, B. Segall, B. K. Meyer, Phys. Rev. B**65**, 075207 (2002).
- [28] M. Goano, F. Bertazzi, M. Penna, E. Bellotti, J. Appl. Phys. **102**, 083709 (2007).
- [29] G. Coli, K. K. Bajaj, Appl. Phys. Lett.**78**, 2861 (2001).
- [30] W. R. L. Lambrecht, S. Limpijumnong, B. Segall, MRS Internet J. Nitride Semicond. Res. 4SI, G6.8 (1999).
- [31] Y. R. Ryu, T. S. Lee, J.A. Lubguban, A. B. Corman, H. W. White, J. H. Leem, M. S. Han, Y. S. Park, C. J. Youn, W. J. Kim, Appl. Phys. Lett. **88**, 052103 (2006).
- [32] X. F. Fan, H. D. Sun, Z. X. Shen, J. L. Kuo, Y. M. Lu, J. Phys: Condens. Matter **20**, 235221 (2008).
- [33] V. Coleman, M. Buda, H. Tan, C. Jagadish, M. Phillips, K. Koike, S. Sasa, M. Inoue, M. Yano, Semicond. Sci. Technol. **21**, L25 (2006).
- [34] N. W. Emanetoglu, S. N. Muthukumar, P. Wu, R. H. Wittstruck, Y. Chen, Y. Lu, IEEE Trans. Ultrason. Ferroelectr. Freq. Contr. **50**, 537 (2003).
- [35] Q. Xu, X. W. Zhang, W. J. Fan, S. S. Li, J. B. Xia, Compos. Mater. Sci. **44**, 72 (2008).
- [36] C. Wang, F. Grillot, J. Even, SPIE Photonics Europe, Brussels, Belgium, (2012).
- [37] G. P. Agrawal, N. K. Dutta, Van Nostrand Reinhold, New York, 240 (1986).

*Corresponding author: talebs2011@hotmail.fr